RESEARCH ARTICLE SUMMARY

ORGANOIDS

# Tissue geometry drives deterministic organoid patterning

N. Gjorevski†, M. Nikolaev†, T. E. Brown†, O. Mitrofanova, N. Brandenberg, F. W. DelRio, F. M. Yavitt, P. Liberali, K. S. Anseth, M. P. Lutolf*

**INTRODUCTION:** Stem cell–derived organoids are in vitro tissue and organ mimetics that have enormous potential as models for human organ development and disease, as platforms for drug discovery and diagnostics, and for the design of cell and gene therapies. However, the stem cell self-organization processes underlying organoid development are poorly controlled, leading to a general lack of reproducibility of most existing organoid cultures. For example, the location and number of crypt-like domains in mouse intestinal organoids—perhaps the best-described organoid system to date—cannot be controlled, nor can the shape, size, and multicellular composition of organoids. The high variability of current organoid models poses a major challenge for basic and translational organoid-based research.

**RATIONALE:** Applying control over organoid formation and the resulting structures would allow both understanding the underlying morphogenetic mechanisms and building models that bear higher likeness to the native counterparts. The final functional architectures of real organs are the product of interplay between epithelial self-organizing programs and extrinsic microenvironmental controllers. Taking inspiration from development in vivo, we complemented organoid self-organization with external regulation. In particular, we have attempted to control the patterning and morphogenesis of intestinal organoids via the physical properties and, in particular, the initial geometry of the tissue itself.

**RESULTS:** We developed bioengineering strategies to extrinsically control the self-organization process of intestinal stem cells through in situ photopatterning of hydrogel mechanics and hydrogel microfabrication. We found that localized patterning of microenvironmental mechanics and predefined hydrogel microtopography could be used to build organoids with a controlled initial size and shape, and we were able to predict and influence the course of their development, especially the number and location of crypt domains. We used the predictability of organoid development to identify the underlying mechanism of epithelial patterning. Our data suggest that in vivo–like tissue geometries can drive stereotypical epithelial patterning by establishing reproducible local differences in cell packing and morphology. These differences in cell shape lead to spatial heterogeneities in YAP mechanosensing/transduction and Notch signaling, which in turn specify "crypt"- and "villus"-like domains by localizing Paneth cell differentiation and suppressing stem cell fates, respectively. Spatial variations in cell morphology dictated by tissue geometry thus render a normally random process highly stereotypical. We exploited these insights to build macroscopic organoids resembling the periodic crypt-villus architecture of the native intestinal epithelium. These structures adopt physiologically accurate patterning and regionalization conferred by tissue geometry only, in the absence of extrinsically imposed biochemical gradients. The predictable and well-delineated villus regions and the accessibility to both the basal and luminal surface are key advantages that enable the study of pathophysiological processes such as intestinal cell shedding.

**CONCLUSION:** We present an approach to guiding stem cell–based organogenesis, a process otherwise driven entirely by "stochastic" self-organization. We also verify long-standing but underexplored paradigms of morphogenesis whereby the present shape of a tissue can help to pattern and specify the course of development, and therefore the future shape, of the tissue. In the case of intestinal crypt formation, we conclude that budding not only can follow Paneth cell appearance but can also precede it. Our organoid cultures can be used to answer questions not readily addressable by existing organoid and animal models, and they may enable the translation of organoid technology to real-world applications. ■

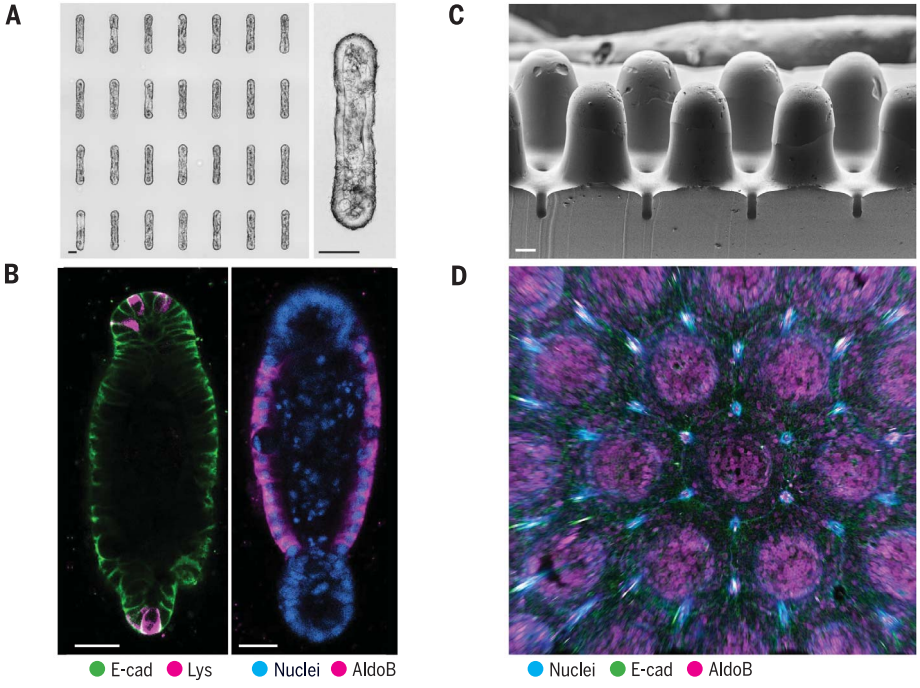


**Extrinsic control of organoid development through engineered microenvironments. (A)** Microengineering-based approaches for controlling the size and shape of intestinal organoids with micrometer-scale precision. (**B**) Organoids of controlled geometry get patterned in a predictable and reproducible manner. (**C** and **D**) Geometry-mediated organoid patterning can be used to produce macroscopic intestinal surfaces with crypt-villus architectures. Organoids are stained for E-cadherin (E-cad), lysozyme (Lys), and aldolase B (AldoB).

The list of author affiliations is available in the full article online.
*Corresponding author. Email: matthias.lutolf@epfl.ch
†These authors contributed equally to this work.
Cite this article as N. Gjorevski *et al.*, *Science* **375**, eaaw9021 (2022). DOI: 10.1126/science.aaw9021

READ THE FULL ARTICLE AT
https://doi.org/10.1126/science.aaw9021

RESEARCH ARTICLE

ORGANOIDS

# Tissue geometry drives deterministic organoid patterning

N. Gjorevski[1]†‡, M. Nikolaev[1]†‡, T. E. Brown[2,3]†, O. Mitrofanova[1], N. Brandenberg[1], F. W. DelRio[4], F. M. Yavitt[2,3], P. Liberali[5], K. S. Anseth[2,3], M. P. Lutolf[1,6]*‡

Epithelial organoids are stem cell–derived tissues that approximate aspects of real organs, and thus they have potential as powerful tools in basic and translational research. By definition, they self-organize, but the structures formed are often heterogeneous and irreproducible, which limits their use in the lab and clinic. We describe methodologies for spatially and temporally controlling organoid formation, thereby rendering a stochastic process more deterministic. Bioengineered stem cell microenvironments are used to specify the initial geometry of intestinal organoids, which in turn controls their patterning and crypt formation. We leveraged the reproducibility and predictability of the culture to identify the underlying mechanisms of epithelial patterning, which may contribute to reinforcing intestinal regionalization in vivo. By controlling organoid culture, we demonstrate how these structures can be used to answer questions not readily addressable with the standard, more variable, organoid models.

Stem cell–derived organoids are in vitro tissue and organ mimetics that hold promise as models of human development and disease, platforms for drug discovery, and material to repair diseased and damaged tissue, including personalized therapies (*1*–*7*). Although organoids display complex architecture and function, the structures generated are often variable, with methods lacking reproducibility. For instance, intestinal organoid formation is largely stochastic, resulting in structures that differ from the native organ in multiple aspects, such as the location and number of crypt-like domains and variation in the shape, size, and cellular composition of the overall organoid. This high variability poses a challenge in basic and translational organoid-based research (*8*, *9*). Although the field of stem cell–based organoids was conceived at least a decade ago and the range of organoid types is continuously expanding, it is only very recently that researchers have introduced methods to control organoid formation (*10*–*15*). Our research group had previously used microfabrication and microfluidics to control the macroscopic shape of intestinal organoids, which ultimately enabled the establishment of long-lived and perfused structures (*13*). This approach used fabrication to form the crypt-villus system, rather than relying on intrinsic morphogenetic programs, such as evagination and budding, which drive both organoid formation and intestinal development in vivo (*16*). However, the mechanisms whereby the macroscopic organoid shape can ultimately pattern the crypt-villus system were not elucidated. In this study, we set out to devise strategies for exerting extrinsic control over intestinal organoid symmetry breaking and crypt formation, and used the resulting models to shed light on the mechanisms by which tissue geometry can regulate intestinal morphogenesis.

[1]Laboratory of Stem Cell Bioengineering, Institute of Bioengineering, School of Life Sciences (SV) and School of Engineering (STI), Ecole Polytechnique Fédérale de Lausanne (EPFL), Lausanne, Switzerland. [2]Department of Chemical and Biological Engineering, University of Colorado, Boulder, CO 80309, USA. [3]BioFrontiers Institute, University of Colorado, Boulder, CO 80303, USA. [4]Material, Physical, and Chemical Sciences Center, Sandia National Laboratories, Albuquerque, NM 87185, USA. [5]Friedrich Miescher Institute for Biomedical Research (FMI), Basel, Switzerland. [6]Institute of Chemical Sciences and Engineering, School of Basic Science (SB), EPFL, Lausanne, Switzerland.
*Corresponding author. Email: matthias.lutolf@epfl.ch
†These authors contributed equally to this work.
‡Present address: Institute for Translational Bioengineering (ITB), Roche Pharma Research and Early Development, Basel, Switzerland.

## Spatiotemporal control over organoid crypt formation by photopatterning

Previously, we showed that the transformation of a round intestinal stem cell (ISC) colony into a crypt-containing organoid within a synthetic hydrogel requires matrix softening (*17*). The global matrix-softening approach we used, however, resulted in stochastic and spatially uncontrolled budding, just as in the conventional organoid cultures that are based on native extracellular matrix (ECM)–derived three-dimensional (3D) matrices (*18*, *19*). We postulated that by introducing localized matrix softening, thus restricting the regions permissive to budding, we might achieve spatially controlled crypt formation.

To this end, we embedded ISC colonies within arginine-glycine-aspartate (RGD)– and laminin-1–containing photosensitive poly(ethylene glycol) (PEG)–based hydrogels (*20*), which undergo degradation and softening when exposed to 405-nm light (fig. S1). Localized light exposure allowed us to introduce softening at predefined regions within the hydrogel surrounding the colony (Fig. 1A). The initial stiffness of the hydrogel matched the value that we previously found to support ISC colony formation but not budding (*17*) (fig. S1), whereas the light dose supplied to specified regions was chosen to effect a drop of stiffness previously identified as crucial for organoid budding (*17*) (Fig. 1B). Shortly (<10 min) after photopatterning, the epithelium adjacent to the softened regions underwent an evagination-like event (movie S1), which we believe to be an attempt to establish mechanical balance. These pseudo-buds continued to extend over the next 72 hours, forming structures that morphologically resembled intestinal crypts (Fig. 1, C to E). Whereas crypt-like buds were frequent within softened regions, they were completely absent outside of these regions. Thus, we were able to control and predict the sites of bud formation with high (84 ± 6%) fidelity (Fig. 1F).

To ensure that the buds were bona fide crypts formed through epithelial symmetry breaking and patterning, rather than merely by differential growth, we considered the distribution of ISCs and differentiated intestinal cells throughout the structure. Lgr5-expressing ISCs were present exclusively at the end of the buds and were absent in the central epithelial cyst (Fig. 1, G and H). Cell division, indicated by incorporation of 5-ethynyl-2′-deoxyuridine (EdU), was similarly localized to crypt structures (Fig. 1I). Likewise, ISC-supporting Paneth cells were present within the buds, whereas enterocytes were confined to the central region of the cyst (Fig. 1, J and K). Enteroendocrine cells were also found within the structures (Fig. 1L). Thus, we used light-mediated matrix softening to control organoid symmetry breaking and direct crypt formation. Of note, the timing of matrix softening is important, because crypt formation was substantially reduced when softening was performed 2 days after the induction of differentiation (fig. S2).

In applying photo-mediated softening to control intestinal organoid formation, we noticed that the symmetry breaking and epithelial patterning were preceded by a change in epithelial shape (movie S1). Specifically, after the rapid evagination-like event that produced nascent buds, the colonies were uniformly composed of ISCs. The budded structure was patterned and transformed into an organoid in the subsequent 24 hours. Bearing in mind that the appearance of the bud preceded the molecular symmetry breaking, we postulated that the bud shape of the crypt epithelium itself represents an integral part of the ISC niche, helping to restrict the ISC zone and establish the crypt-villus axis. Indeed, our recent work demonstrated that ISCs grown in crypt-shaped cavities within microfluidic scaffolds can be

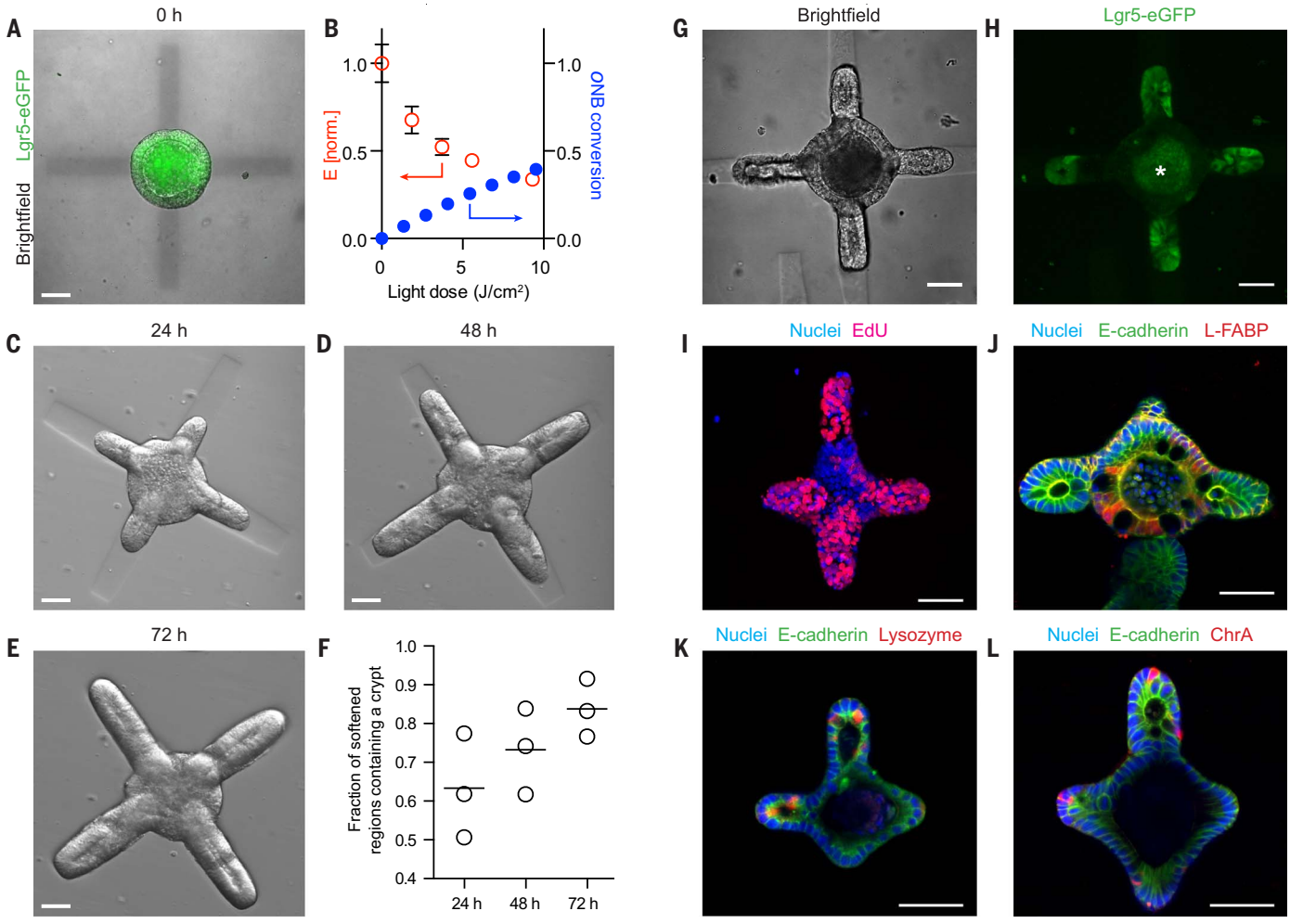


**Fig. 1. Spatiotemporal control over organoid crypt formation through photopatterning.** (**A**) Composite image showing Lgr5-GFP expression in a symmetric colony and photopattern visible with transmitted 405-nm light immediately after spatially restricted light exposure. (**B**) Mechanical characterization of hydrogels with atomic force microscopy reveals that the reduction in the Young's modulus (E) corresponds to conversion of photocleavable *ortho*-nitrobenzyl (*o*NB) moieties within the gel. Error bars denote SD. (**C** to **E**) Spatially defined crypt formation within photopatterned gels 24 hours (C), 48 hours (D), and 72 hours (E) after light-induced softening. (**F**) Quantification of fraction of photo-softened gel regions containing a crypt. Individual data points and mean are shown. (**G** to **I**) Lgr5-eGFP expression [(G), (H)] and proliferation (I) are localized within the buds, extending into the softened regions. (**J**) Enterocytes (L-FABP stain) are found in the central regions of the organoids. (**K**) Paneth cells (lysozyme stain) are restricted to the buds of the organoids. (**L**) Enteroendocrine cells (ChrA stain) are also present without clear morphological localization, consistent with their distribution in the real intestine. Scale bars, 30 μm.

maintained in long-term cultures (*13*), which suggests that tissue shape directly influences patterning. To test this hypothesis, we set out to build intestinal tissues of predefined size and geometry that mimic those of the crypt, and to monitor how the initial shape affects the spatial distributions of ISCs and the various differentiated cell types within the tissue (Fig. 2).

### Microfabricated intestinal organoids of controlled geometry

We used soft lithography to microstructure a 3D hydrogel [composed of type I collagen (3 mg/ml) and 25% (v/v) Matrigel] with cavities of defined size and shape (*21*, *22*), which were subsequently filled with purified Lgr5-eGFP$^+$ ISCs (Fig. 2A). Initially randomly dispersed, the stem cells began to form contacts with each other and the surrounding matrix, and within 48 hours they self-organized into a lumenized epithelial tissue conforming to the shape of the preexisting cavity. We used this approach to form 3D intestinal tissues of arbitrary sizes and shapes (fig. S3, A to C). Next, we sought to determine whether the differentiation of the engineered intestinal tissues followed a stereotypical pattern or occurred randomly. The method described above generates hundreds of regularly spaced tissues of identical size and shape, which permits rapid imaging of fluorescent markers or proteins visualized by immunofluorescence analysis, as well as quantification by automated image segmentation and analysis (fig. S3D). Stacking images of a high number (>80) of individual tissues in registration can provide information about the average distribution of the molecular marker of interest, with high statistical confidence (fig. S3D). Although the tissues were formed from a cell suspension uniformly expressing Lgr5-eGFP, we found that within 4 days of culture, the signal became restricted to the curved ends of the tissues (Fig. 2, B and C), indicating that ISCs are confined to these regions in a pattern similar to that of the native crypt. The microfabricated tissues proceeded to extend crypt-like buds with a spatial bias reflecting that of Lgr5 expression: The curved ends of the tissues were significantly more likely to extend buds than the flat sides (Fig. 2, D and E). The spatial patterning also extended to differentiated intestinal cell types. Immunofluorescence analysis for Paneth cells and enterocytes revealed that the former

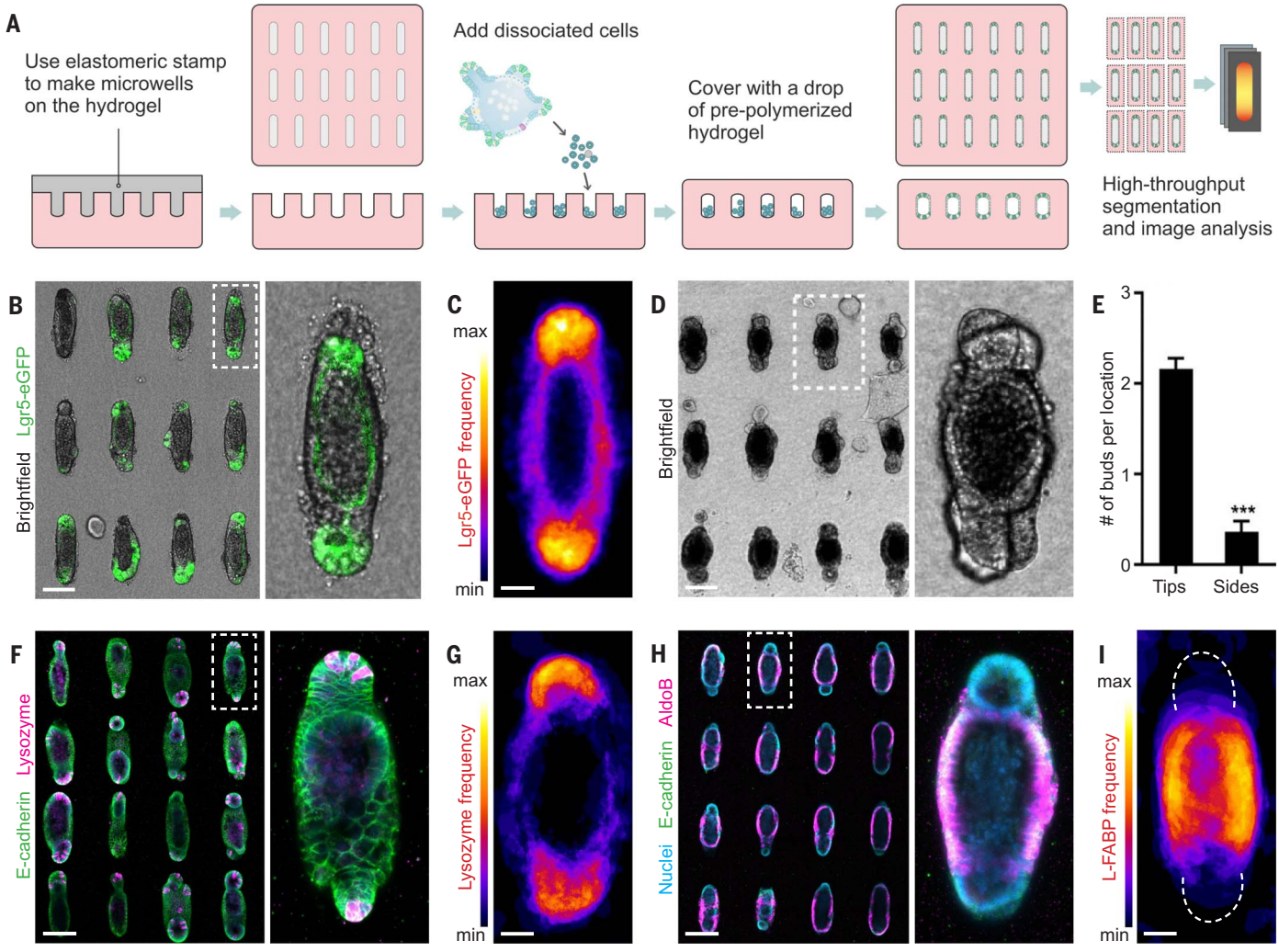


**Fig. 2. Geometrically controlled symmetry breaking and epithelial patterning within intestinal organoids.** (**A**) Schematic depicting the generation of microfabricated tissues of controlled size and shape. (**B**) An array of intestinal organoids formed from engineered intestinal tissues of rodlike geometry and magnification. (**C**) Frequency map showing average Lgr5 expression over ~80 tissues. (**D** and **E**) An array of intestinal organoids at day 5 (D) and quantification of the average number of buds per location (E) within tubular intestinal tissues. ***$P < 0.001$. (**F** and **G**) Paneth cell staining by lysozyme in the array of intestinal organoids (F) and average Paneth cell distribution (G). (**H** and **I**) AldoB-expressing enterocytes within rod-shaped organoids (H) and average enterocyte distribution (I). The dashed lines indicate the average contour of the tissues. Scale bars, 100 μm [(B), (D), (F), (H)], 25 μm [(C), (G), (I)].

were preferentially localized to the same end-locations as the ISCs (Fig. 2, F and G), whereas the latter were on average excluded from the ends and confined to the middle of the tissue (Fig. 2, H and I). These findings suggest that the spatial distribution of ISCs and differentiated cells within the engineered microtissues reflects the patterning of the crypt-villus axis in vivo (*23*). Thus, we could predict and control the site of budding and crypt formation within the organoids by merely manipulating their initial geometry.

### Mechanism of geometry-controlled epithelial patterning

To elucidate how the initial epithelial geometry might dictate the patterning of intestinal tissue, we monitored the process using time-lapse microscopy (Fig. 3, A to D, and movie S2). Lgr5 expression at the time of seeding and shortly thereafter (<2 hours) appeared uniformly low. As the organoids formed in the crypt-like space, Lgr5 was reexpressed strongly at the ends of tissues, remaining low elsewhere (Fig. 3, C and D). Before the Lgr5 regionalization, we observed a morphological difference between the curved end regions and the flat sides. Within 24 hours of culture, and owing likely to crowding due to proliferation within a limited space at the ends, the cells in these regions became more packed, whereas cells in the lateral regions remained spread and flattened (Fig. 3E). Indeed, measurement of the internuclear distance at the different regions revealed a significant difference in cell packing (Fig. 3F).

Yes-associated protein 1 (YAP) is a regulator of ISC fate (*24*–*27*), which is strongly influenced by cell shape and mechanics (*28*, *29*). To ascertain whether the differences in cell morphology between the different regions correlated with differences in YAP activity, we analyzed the subcellular distribution of YAP. Shortly after seeding, YAP was uniformly nuclear throughout the tissue, except in some cases where cell crowding was observed early in the curved regions as a result of (stochastic) variations in cell density (fig. S4A). Between 12 and 24 hours after seeding, corresponding to the time when spatial differences in cell shape appear (and preceding the patterning of Lgr5), nuclear YAP localization became restricted to the lateral regions of the tissues. At the ends of the tissues, cytoplasmic translocation, and

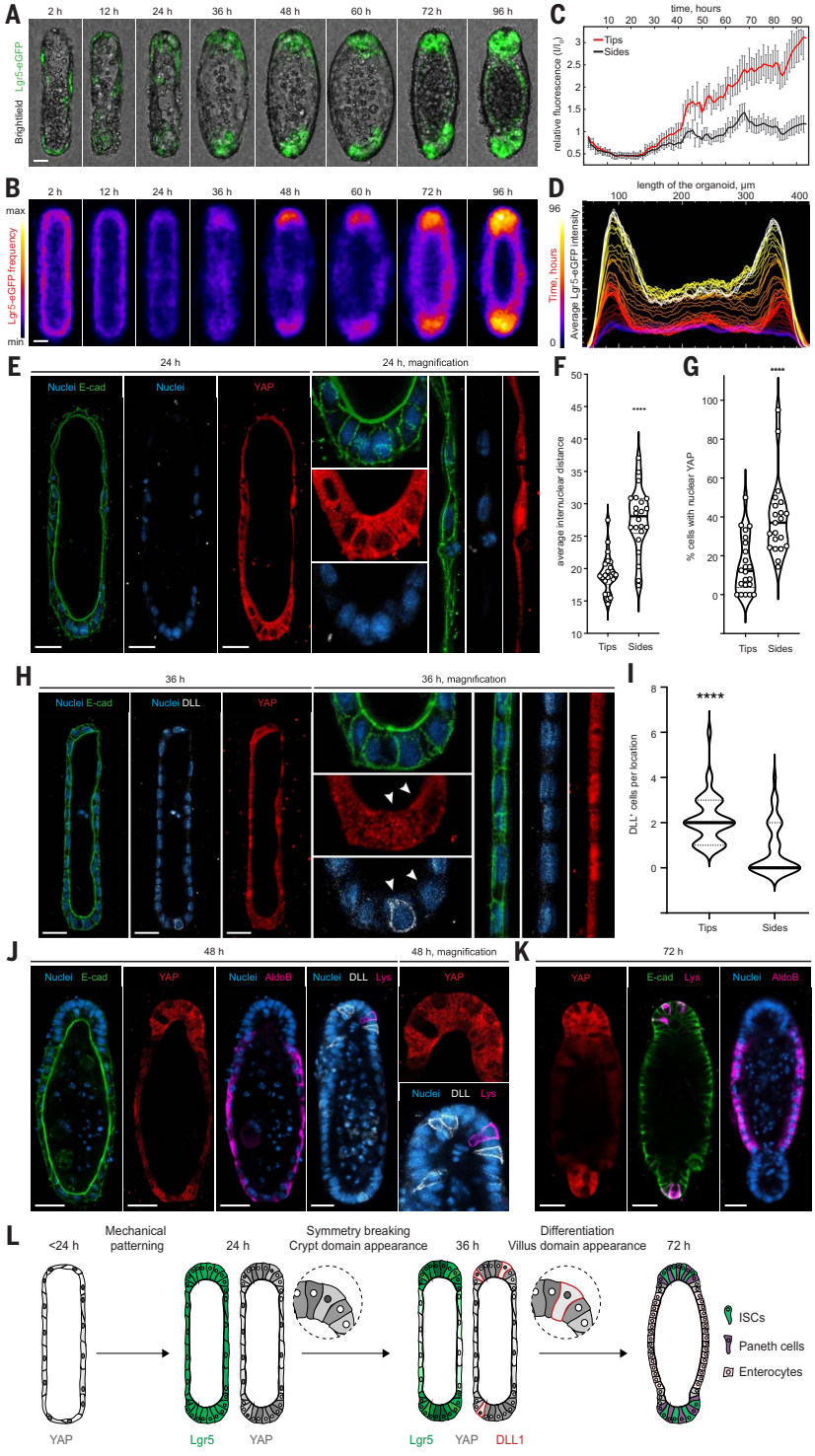


**Fig. 3. Tissue geometry controls organoid patterning through cell shape–mediated regulation of YAP and Notch signaling.**
(**A** and **B**) Bright-field and Lgr5-eGFP time-lapse imaging of the representative organoid development (A) and frequency maps showing average Lgr5 expression over ~80 tissues (B). (**C** and **D**) Relative changes in the Lgr5-eGFP expression in curved ends and flat sides of the organoids over time (C) and Lgr5-eGFP localization along length of the averaged tissue over time (D). (**E**) Immunofluorescence images showing the difference in internuclear distance, cell shape, and subcellular distribution of YAP between cells of the end and the side regions, 24 hours after cell loading. (**F**) Quantification of internuclear distance within the end and side regions of the tissues. Individual points, which represent the distance between neighboring nuclei, and means are shown. (**G**) Quantification of the nuclear localization of YAP within cells of the different organoid regions. Individual points and means are shown. (**H**) Immunofluorescence images showing the difference in the subcellular distribution of YAP cells between cells of the end and the side regions and appearance of the first DLL$^+$, 36 hours after cell loading. Arrowheads denote adjacent pairs of YAP-ON/OFF cells; the YAP-ON cell expresses DLL1. (**I**) Quantification of DLL$^+$ cell localization. (**J** and **K**) Immunofluorescence images showing YAP expression and localization of the enterocytes (AldoB), Paneth cells (Lys), and DLL$^+$ cells in the representative organoids. (**L**) Schematic illustration summarizing the proposed mechanism of the geometry-driven organoid patterning. Scale bars, 25 µm. ****$P$ < 0.0001 [(F), (G), (I)].

therefore inactivation, was observed (Fig. 3, E and G). This geometry-dependent regionalization of YAP activity was again lost at later time points (>36 hours) when cells throughout the tissue became uniformly packed (fig. S4A). To test whether differential cell spreading (and, conversely, cell crowding) is sufficient to drive differences in YAP activity, we cultured ISCs at equal cell-seeding density in microcavities of small (50 µm) and large (100 µm) diameter, resulting in a packed or a spread system (fig. S4B). YAP activity strongly correlated with cell spreading: Nuclear translocation was significantly more frequent within 100-µm wells than in 50-µm wells, which suggests that tissue geometry per se controls the spatially patterned activation of YAP through differential cell spreading (fig. S4, C and D).

Several recent studies have implicated YAP activation in the repression of canonical ISC signatures, including *Lgr5*, *Olfm4*, and *EphB3*, during intestinal regeneration and cancer (*24*, *27*, *30*, *31*). Given the spatial and temporal correlation between YAP induction and Lgr5 suppression, we hypothesized that the patterning of this system is driven by geometrically and mechanically established gradients in

YAP activity. In line with this model, abrogating spatial gradients in YAP activity by uniform induction [via treatment with the MST1/2 signaling inhibitor XMU-MP-1 (*32*)] or inhibition [via treatment with verteporfin (*33*, *34*)] both resulted in loss of intestinal tissue patterning (fig. S4, E to G). Furthermore, blocking cell spreading and the formation of mechanical gradients by treatment with the contractility inhibitor blebbistatin (*29*, *35*) abolished the patterns of both YAP activity and intestinal cell fate (fig. S5). A 36-hour delay of blebbistatin treatment did not interfere with Lgr5 patterning (fig. S5A); during this 36-hour period, treatment was most efficient only within a short time window in which the geometry-controlled cell spreading resulted in differential YAP activation (fig. S5, B and C). Thus, these gain- and loss-of-function experiments show that an early, geometrically induced YAP prepattern is necessary to promote later tissue regionalization. Previous studies by us and others have hinted that spatial heterogeneities in YAP are required for intestinal tissue morphogenesis (*17*, *30*). Here, we have shown that these heterogeneities can be governed by geometrically established gradients in cell mechanics to control downstream tissue patterning.

To explore whether the finding of geometrically and mechanically mediated YAP patterning translates to human intestinal epithelium, we generated arrays of human small intestinal organoids (fig. S6, A and B). The spatial gradients of YAP activity described above were also present in the human system and followed a similar temporal profile (fig. S6, C and D). Note, however, that the human organoids of controlled shape did not proceed to self-organize into a crypt-villus structure (fig. S6E). It is likely that the current culture conditions do not support robust Paneth cell differentiation and ISC niche establishment.

After determining that symmetry breaking in the system likely occurs through YAP-mediated spatial restriction of ISC maintenance, we wanted to further explore how the ISC niche at the ends is established. Multiple studies have shown that Paneth cells provide essential support to ISCs within intestinal organoids, and that their appearance is crucial for the establishment of the ISC niche (*18*, *19*, *30*, *36*). Recent work by Serra *et al.* revealed a YAP-Notch symmetry-breaking mechanism that is responsible for Paneth cell appearance and crypt initiation in classical intestinal organoids (*30*). In particular, it was found that Paneth cell differentiation and crypt initiation occur exactly at the sites where YAP ON cells are adjacent to YAP OFF cells. Bearing in mind the pattern of YAP activity described above, we reasoned that the ends of the tissue are the regions where YAP OFF and YAP ON cell pairs are more likely to coexist, triggering YAP-Notch symmetry breaking. In this model, an early indication of Paneth cell differentiation is the expression of the Notch ligand DLL1 (delta-like ligand 1) in cells featuring inactive Notch and active YAP. We observed the appearance of this cell type at the end of the tissue around 36 hours (Fig. 3, H and I), along with localized Notch activation, as evidenced by the presence of the Notch intracellular domain (NICD) (fig. S7, A and B). Consistently with this model, Paneth cells were observed at these regions within 48 hours of culture (Fig. 3, J and K). Localized Notch activation and Paneth cell appearance were required for durable tissue patterning: Uniform inhibition of Notch by treatment with the γ-secretase inhibitor DAPT abolished patterns in Lgr5 and Paneth cell differentiation (fig. S7, C to E), as did treatment with valproic acid (fig. S7F), which, although a known pleiotropic histone deacetylase inhibitor, has been shown to activate Notch in this system (*37*). Taken together, these data show that the tissue shape leads to a mechanically controlled prepatterning of epithelial cells with different YAP activity, which in turn results in (i) suppression of crypt cell fates at the sides of the tissues and (ii) a stereotypical Notch-DLL1 lateral inhibition event at the ends, driving the formation of the first Paneth cell that constitutes the niche (movie S3; proposed mechanism summarized in Fig. 3L).

In this system, Wnt is likely a crucial factor in maintaining and reinforcing the cell fate pattern. Indeed, we believe that it is the Wnt (and Notch) ligands produced by the first Paneth cells appearing at the tips of the tissues that help locally establish and maintain the stem cell niche. In line with this model, inhibition of Wnt production and secretion by treatment with IWP2 depletes $Lgr5^+$ ISCs from the tips and abolishes niche appearance at 36 hours of culture and beyond (fig. S8A). Compensating for the blocked Wnt production by supplementing with exogenous Wnt3a led to the expected outcome: $Lgr5^+$ ISCs were no longer depleted from the system at 36 hours, but were distributed more uniformly throughout the tissue (fig. S8B). Exposure to exogenous Wnt3a in the absence of IWP2 did not significantly affect patterning (fig. S8C). These data support the role of localized Wnt production and signaling as an important factor in establishing and maintaining the patterning in the system. However, we believe that localized Wnt signaling, although necessary, is not sufficient to drive symmetry breaking in the tissues. Monitoring the Wnt activity within the tissues, we found that the restriction of Wnt signaling followed rather than preceded the patterning of Notch, Lgr5, and Paneth cells (Fig. 3L and fig. S8, G and H).

In addition to the mechanism introduced, we also considered others that had previously been described for the regionalization of intestinal and other epithelia. Investigating the potential role of geometrically established inhibitory gradients in sonic hedgehog (SHH) (*38*) or transforming growth factor–β (TGF-β) (*21*) (fig. S9), as well as the role of patterning through cell-cell repulsive interactions (*39*–*41*) (fig. S10), we found that, whereas these mechanisms may contribute to or reinforce the patterning, they are likely not responsible for the initial symmetry breaking.

### Bioengineered tissues with an in vivo–like tissue architecture and pattern

Next, intrigued by the possibility that differences in the packing of cells inside and outside the intestinal crypt may help to locate ISCs at the bottom of the crypt and establish a crypt-villus–like axis, we used a simplified intestinal surface with indentations that mimic the size and shape of the crypt, surrounded by flat regions that approximate the much larger surface of the villi (fig. S11). Moving from the bottom of the engineered crypts to the exterior surfaces (at 24 to 36 hours after cell loading), we observed a gradual increase in cell spreading and YAP activation (movie S4). Conversely, Lgr5 expression was maximal at the bottom of the crypts and was virtually absent outside of the cavities, indicating that stem cells were preserved only at the bottom of the crypts, in the familiar in vivo–like pattern (fig. S11B), despite a homogeneous cocktail of soluble cell fate–determining factors.

Finally, we sought to exploit these mechanistic insights to engineer macroscopic organoids with an in vivo tissue architecture (Fig. 4). We microfabricated hydrogel substrates resembling the native intestinal mucosa, with crypts at the bottom and villi protruding outward (Fig. 4, A to D). Within 48 hours, ISCs seeded on these scaffolds expanded to establish a confluent monolayer of cells (Fig. 4E and movie S5). Induction of differentiation resulted in highly stereotyped organoid patterning, with stem cell–containing crypts (Fig. 4F) interspersed with villi composed of enterocytes and other differentiated cell types (Fig. 4G and fig. S12). These results demonstrate that the principles controlling cell fate patterning at the subtissue scale can be harnessed to engineer macroscopic intestinal surfaces that capture the cellular organization and periodicity of the crypt-villus system. Previous attempts to engineer intestinal surfaces (*10*, *11*) were dependent on complex chemical gradients to induce patterning (i.e., did not reveal or exploit tissue geometry as a patterning cue) and have not demonstrated recapitulation of the multicellular organization and periodicity of the in vivo crypt-villus system. A key advantage of the engineered crypt-villus surfaces over 3D organoids is the well-delineated and mature villus region and accessibility to the luminal intestinal surface. We leveraged

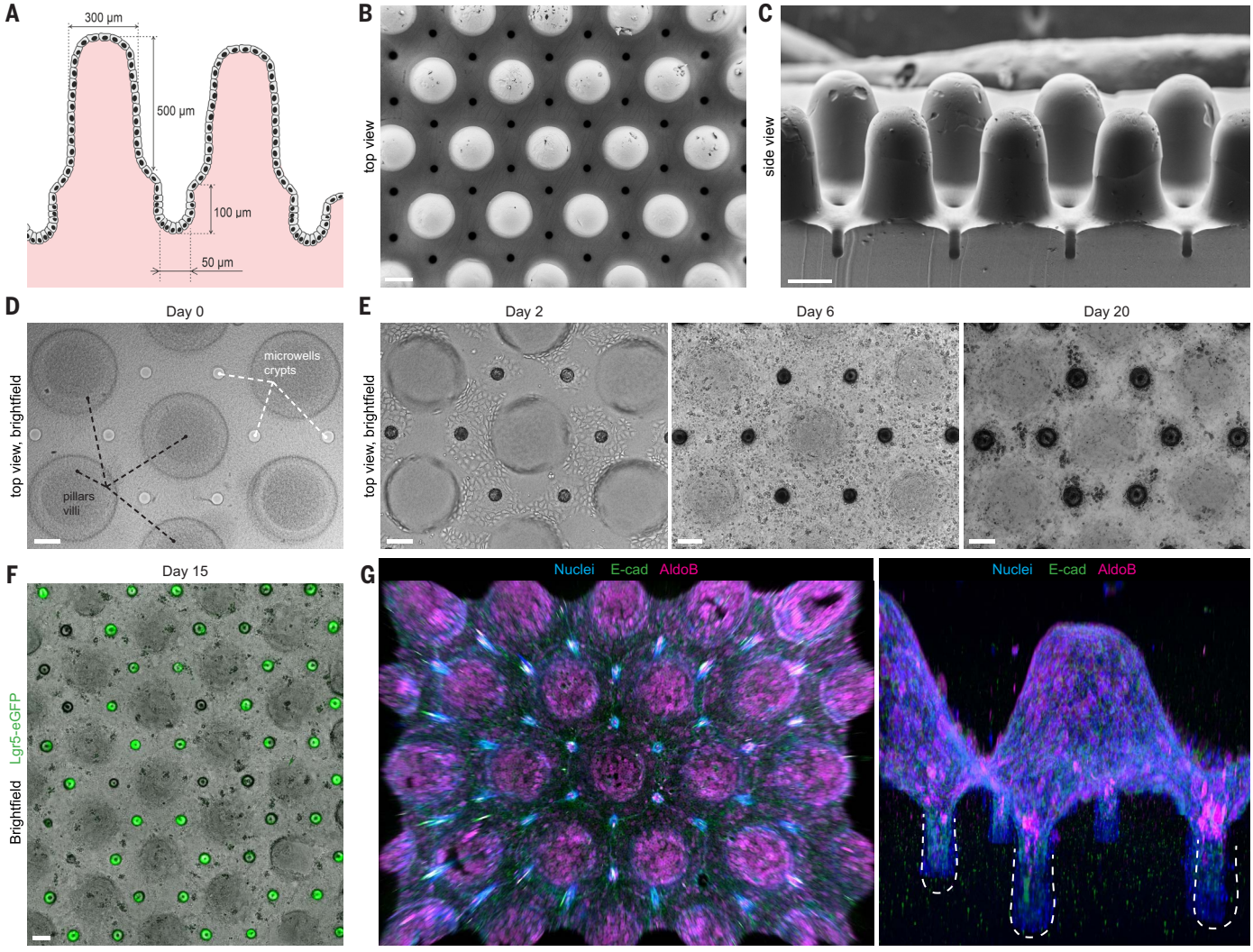


**Fig. 4. Bioengineered organoids with an in vivo–like tissue architecture.** (**A**) Scheme of the designed topography resembling the native tissue with characteristic intestinal crypt-villus architecture. (**B** and **C**) SEM images of the poly(dimethylsiloxane) (PDMS) template used for fabricating bioengineered hydrogel substrates featuring a crypt-villus architecture (top and side views, respectively). Scale bars, 200 µm. (**D**) Top view of the hydrogel substrate shaped according to the topology of the native intestinal mucosa. (**E**) Bright-field time-course images of the intestinal epithelium development. (**F**) Localization of the Lgr5$^{+}$ stem cells in the engineered crypts. In (D) to (F), extended depth of field for a z-stack ~ 600 µm; scale bars, 100 µm. (**G**) 3D reconstruction of the immunofluorescence images, showing confluent monolayer of E-cadherin–expressing epithelial cells covering hydrogel substrates, harboring villi composed of enterocytes (AldoB). See movie S5 for full time course of the epithelium growth and 3D immunofluorescence imaging.

these features, along with the possibility of live imaging, to explore the process of intestinal shedding.

Shedding is an important physiological process, whereby the pressure due to proliferative overcrowding is relieved while maintaining a tight and functional intestinal epithelial barrier. When dysregulated in pathological situations, such as inflammatory disease, shedding leads to loss of barrier function, exacerbating the disease (*42*, *43*). Intestinal epithelial cell death and extrusion from the epithelium has been difficult to study in vitro, for the reasons mentioned above, whereas fixed ex vivo intestinal sections capture only snapshots of the process, precluding study of the temporal dynamics. We observed cell shedding within our engineered intestinal epithelia (Fig. 5 and movie S6) and showed that the process recapitulated pathophysiological hallmarks of the in vivo process. First, we found that cell shedding was always associated with the appearance of an actin ring at the interface of the shed cell and its neighbors (Fig. 5A and movie S7) (*44*, *45*). Second, the system replicated the extensive shedding induced by the inflammatory cytokine tumor necrosis factor–α (TNF-α) (Fig. 5B), which has been shown to lead to loss of barrier function during intestinal inflammation (*42*, *46*). Unlike 3D organoids and ex vivo approaches, our system allows the collection of shed cells for downstream analysis (Fig. 5C). We followed shed cells continuously before, during, and after extrusion and monitored apoptosis simultaneously. Using this approach, we demonstrated that apoptosis can occur before shedding, in situ, as well as after the cell has been extruded from the epithelium (Fig. 5D and movie S8).

We thus report a means to engineer external guidance in stem cell–based organogenesis, a process otherwise fully driven by stochastic self-organization. We show that localized patterning of ECM mechanics and topographically structured hydrogel scaffolds can be used to build organoids of a controlled initial size and shape and to predict and influence the course of their development, in particular the breaking of symmetry and the number and location of crypt-like domains. This advance may help to overcome the lack of reproducibility

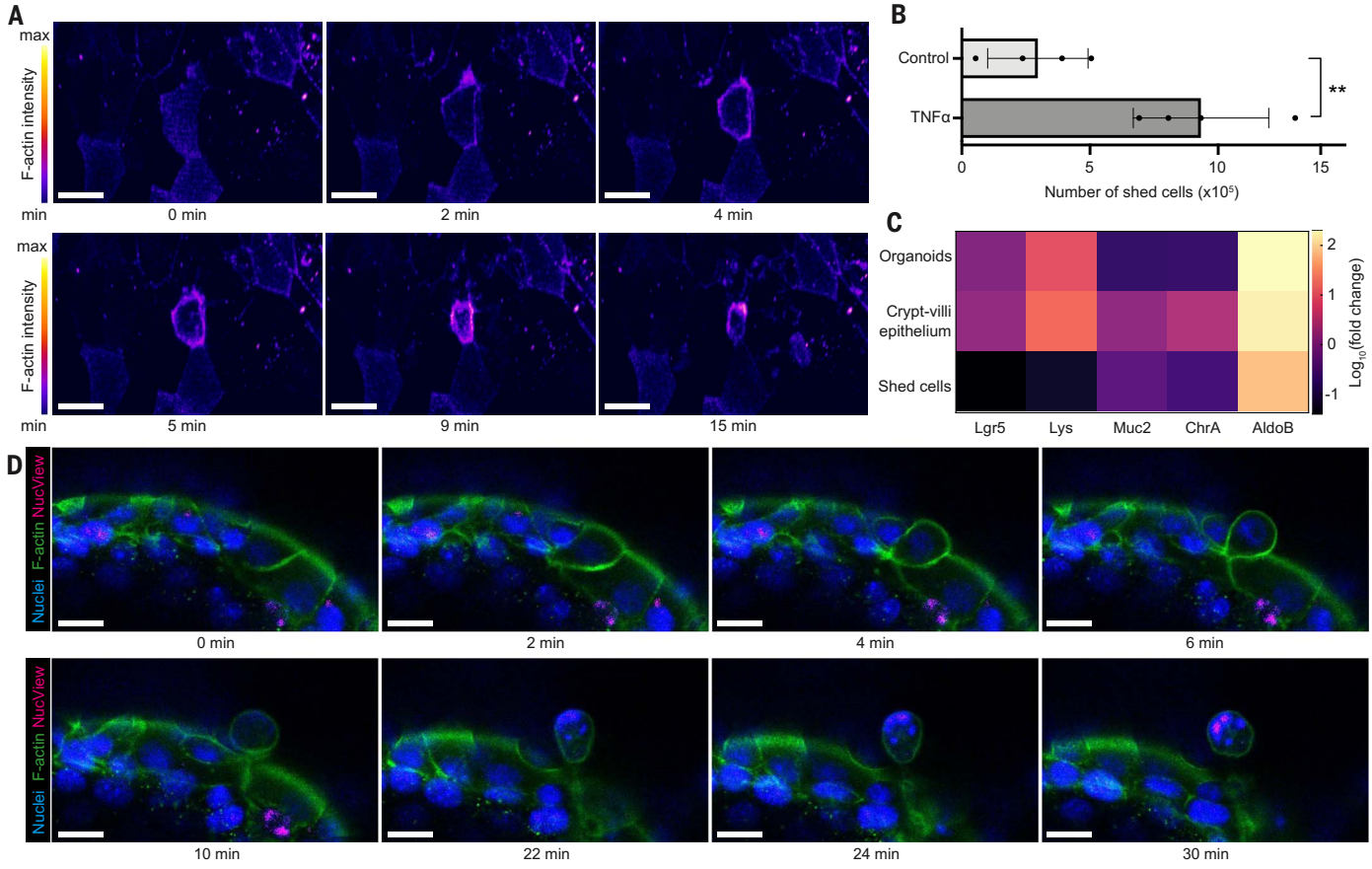


**Fig. 5. Leveraging a bioengineered crypt-villus system to study the mechanisms of epithelial cell shedding in the small intestine.** (**A**) Time-course imaging of epithelial cell undergoing shedding from the villus tip reveals gradual contraction of the of F-actin ring at the interface of the shed cell and its neighbors. (**B**) Quantification of the number of cells shed under homeostatic conditions and after treatment with TNF-α. Individual points and means with SD are shown. $^{**}P$ = 0.0025. (**C**) Heatmap of quantitative real-time PCR data showing the relative expression of intestine-specific genes (Lgr5, Lys, Muc2, ChrA, AldoB) in organoids, 15-day-old engineered crypt-villus epithelia, and shed cells over 8 hours. Data are average expression over $n$ = 3 samples. (**D**) Time-course fluorescence imaging identifies caspase-3/7 activation after cell extrusion from the villus tip. See movies S6 to S8 for full time-lapse imaging of the shedding. Scale bars, 20 μm.

and control that are major limitations of organoids, undercutting their utility in basic and translational research. The controlled organoid development afforded by these approaches allowed us to identify a role for tissue geometry in intestinal tissue patterning, and to dissect the underlying mechanisms. Our data suggest that anisometric tissue geometries drive stereotypic epithelial patterning by establishing reproducible local differences in cell packing and morphology. It is the heterogeneities in YAP activity that ultimately prescribe "villus" and "crypt" domains by suppressing stem cell fates and localizing Notch-mediated Paneth cell differentiation, respectively. We believe that spatial variations in cell morphology alone are likely sufficient to induce symmetry breaking, and could be responsible for driving crypt initiation within classical organoids, where they would occur randomly. We have shown that tissue geometry can be used as a means to deterministically control the spatial distribution of cell morphology and, consequently, cell fate. The notion that morphogenesis is self-referential—that tissue form can serve as an independent input into its further development—is not new (*21*, *47*). In the case of the native intestine, the shape of the villi has been shown to influence the restriction of the stem cell zones by introducing diffusion-based spatial heterogeneities in signals communicated between the epithelium and the mesenchyme (*38*). Our experiments reveal that ISC restriction to the ends of crypt-like engineered tissue occurs in the absence of villi and mesenchyme; this suggests a complementary mechanism for intestinal regionalization, whereby the epithelial geometry per se allows for autonomous patterning of the tissue.

## Methods summary

A full description of materials and methods is provided in the supplementary materials. Briefly, for organoid photopatterning experiments, ISC colonies were embedded within RGD- and laminin-1–containing photosensitive poly(ethylene glycol) (PEG)–based hydrogels (*20*), which undergo degradation and softening when exposed to 405-nm light. Photodegradation was performed on a laser scanning microscope (Zeiss LSM 710, 405-nm laser at a power of 1 mW) using four ROIs approximating the in vivo crypt dimensions (20 μm × 300 μm) arranged in a cross shape around the colony in a single plane. Approximately 30 colonies per gel were patterned and then the hydrogel was placed in differentiation medium (EGF, Noggin, and R-spondin) to induce differentiation and crypt-villus patterning.

Arrays of the microfabricated intestinal organoids were created using elastomeric stamps [PDMS, poly(dimethylsiloxane)] containing the desired geometries in bas relief. A hydrogel composed of type I collagen and 25% (v/v) Matrigel was cast on the bottom of the cell culture plate between two thin parallel PDMS spacers. A PDMS stamp with cavities of defined size and shape was placed on top of the PDMS spacers and hydrogel was polymerized in the incubator for 30 min. After removal of the stamp, hydrogels were covered with Advanced

DMEM:F12 medium and stored in the incubator. Intestinal organoids were cultured in Matrigel following previously published protocols (*37*). For cell loading in the microwells, concentrated suspension of dissociated intestinal stem cells was pipetted on top of the hydrogel surface. Cells were allowed to sediment within the microcavities of the gels for 5 to 7 min, and nonadherent cells were gently washed with medium. Partially gelled collagen "lid" was placed on top of the cell arrays and the two layers of collagen were allowed to seal for additional 15 min in the incubator. ISC expansion medium supplemented with 2.5 μM thiazovivin was added. The cells were allowed to self-organize into lumenized epithelial stem cell colonies adopting the geometry of the hydrogel microwells (typically 36 hours). To induce differentiation, budding, and organoid formation, the medium was replaced with fresh medium containing EGF, Noggin, and R-spondin.

Microfabricated crypt arrays and crypt-villi–shaped epithelium were produced in an identical manner, but the patterns were not sealed with a second layer of hydrogel and therefore cells were permitted to grow both within the cavities and atop the external surfaces.

## REFERENCES AND NOTES


1. H. Clevers, Modeling Development and Disease with Organoids. *Cell* **165**, 1586–1597 (2016). doi: 10.1016/j.cell.2016.05.082; pmid: 27315476
2. J. Drost, H. Clevers, Organoids in cancer research. *Nat. Rev. Cancer* **18**, 407–418 (2018). doi: 10.1038/s41568-018-0007-6; pmid: 29692415
3. J. Drost *et al*., Use of CRISPR-modified human stem cell organoids to study the origin of mutational signatures in cancer. *Science* **358**, 234–238 (2017). doi: 10.1126/science.aao3130; pmid: 28912133
4. M. A. Lancaster, J. A. Knoblich, Organogenesis in a dish: Modeling development and disease using organoid technologies. *Science* **345**, 1247125 (2014). doi: 10.1126/science.1247125; pmid: 25035496
5. G. Vlachogiannis *et al*., Patient-derived organoids model treatment response of metastatic gastrointestinal cancers. *Science* **359**, 920–926 (2018). doi: 10.1126/science.aao2774; pmid: 29472484
6. G. Rossi, A. Manfrin, M. P. Lutolf, Progress and potential in organoid research. *Nat. Rev. Genet.* **19**, 671–687 (2018). doi: 10.1038/s41576-018-0051-9; pmid: 30228295
7. Y. Sasai, Cytosystems dynamics in self-organization of tissue architecture. *Nature* **493**, 318–326 (2013). doi: 10.1038/nature11859; pmid: 23325214
8. M. Huch, J. A. Knoblich, M. P. Lutolf, A. Martinez-Arias, The hope and the hype of organoid research. *Development* **144**, 938–941 (2017). doi: 10.1242/dev.150201; pmid: 28292837
9. Advances in Organoid Technology: Hans Clevers, Madeline Lancaster, and Takanori Takebe [edited interview with Clevers, Lancaster, and Takebe]. *Cell Stem Cell* **20**, 759–762 (2017). doi: 10.1016/j.stem.2017.05.014
10. Y. Wang *et al*., A microengineered collagen scaffold for generating a polarized crypt-villus architecture of human small intestinal epithelium. *Biomaterials* **128**, 44–55 (2017). doi: 10.1016/j.biomaterials.2017.03.005; pmid: 28288348
11. R. Kim *et al*., Formation of arrays of planar, murine, intestinal crypts possessing a stem/proliferative cell compartment and differentiated cell zone. *Lab Chip* **18**, 2202–2213 (2018). doi: 10.1039/C8LC00332G; pmid: 29944153
12. Y. Wang *et al*., Formation of Human Colonic Crypt Array by Application of Chemical Gradients Across a Shaped Epithelial Monolayer. *Cell. Mol. Gastroenterol. Hepatol.* **5**, 113–130 (2017). doi: 10.1016/j.jcmgh.2017.10.007; pmid: 29693040
13. M. Nikolaev *et al*., Homeostatic mini-intestines through scaffold-guided organoid morphogenesis. *Nature* **585**, 574–578 (2020). doi: 10.1038/s41586-020-2724-8; pmid: 32939089
14. M. A. Lancaster *et al*., Guided self-organization and cortical plate formation in human brain organoids. *Nat. Biotechnol.* **35**, 659–666 (2017). doi: 10.1038/nbt.3906; pmid: 28562594
15. H. M. Poling *et al*., Mechanically induced development and maturation of human intestinal organoids in vivo. *Nat. Biomed. Eng.* **2**, 429–442 (2018). doi: 10.1038/s41551-018-0243-9; pmid: 30151330
16. M. Zinner, I. Lukonin, P. Liberali, Design principles of tissue organisation: How single cells coordinate across scales. *Curr. Opin. Cell Biol.* **67**, 37–45 (2020). doi: 10.1016/j.ceb.2020.07.004; pmid: 32889170
17. N. Gjorevski *et al*., Designer matrices for intestinal stem cell and organoid culture. *Nature* **539**, 560–564 (2016). doi: 10.1038/nature20168; pmid: 27851739
18. T. Sato *et al*., Single Lgr5 stem cells build crypt-villus structures in vitro without a mesenchymal niche. *Nature* **459**, 262–265 (2009). doi: 10.1038/nature07935; pmid: 19329995
19. T. Sato, H. Clevers, Growing self-organizing mini-guts from a single intestinal stem cell: Mechanism and applications. *Science* **340**, 1190–1194 (2013). doi: 10.1126/science.1234852; pmid: 23744940
20. D. D. McKinnon, T. E. Brown, K. A. Kyburz, E. Kiyotake, K. S. Anseth, Design and characterization of a synthetically accessible, photodegradable hydrogel for user-directed formation of neural networks. *Biomacromolecules* **15**, 2808–2816 (2014). doi: 10.1021/bm500731b; pmid: 24932668
21. C. M. Nelson, M. M. Vanduijn, J. L. Inman, D. A. Fletcher, M. J. Bissell, Tissue geometry determines sites of mammary branching morphogenesis in organotypic cultures. *Science* **314**, 298–300 (2006). doi: 10.1126/science.1131000; pmid: 17038622
22. C. M. Nelson, J. L. Inman, M. J. Bissell, Three-dimensional lithographically defined organotypic tissue arrays for quantitative analysis of morphogenesis and neoplastic progression. *Nat. Protoc.* **3**, 674–678 (2008). doi: 10.1038/nprot.2008.35; pmid: 18388950
23. H. Clevers, The intestinal crypt, a prototype stem cell compartment. *Cell* **154**, 274–284 (2013). doi: 10.1016/j.cell.2013.07.004; pmid: 23870119
24. A. Gregorieff, Y. Liu, M. R. Inanlou, Y. Khomchuk, J. L. Wrana, Yap-dependent reprogramming of Lgr5$^+$ stem cells drives intestinal regeneration and cancer. *Nature* **526**, 715–718 (2015). doi: 10.1038/nature15382; pmid: 26503053
25. M. Imajo, M. Ebisuya, E. Nishida, Dual role of YAP and TAZ in renewal of the intestinal epithelium. *Nat. Cell Biol.* **17**, 7–19 (2015). doi: 10.1038/ncb3084; pmid: 25531778
26. T. Panciera, L. Azzolin, M. Cordenonsi, S. Piccolo, Mechanobiology of YAP and TAZ in physiology and disease. *Nat. Rev. Mol. Cell Biol.* **18**, 758–770 (2017). doi: 10.1038/nrm.2017.87; pmid: 28951564
27. S. Yui *et al*., YAP/TAZ-Dependent Reprogramming of Colonic Epithelium Links ECM Remodeling to Tissue Regeneration. *Cell Stem Cell* **22**, 35–49.e7 (2018). doi: 10.1016/j.stem.2017.11.001; pmid: 29249464
28. S. Dupont *et al*., Role of YAP/TAZ in mechanotransduction. *Nature* **474**, 179–183 (2011). doi: 10.1038/nature10137; pmid: 21654799
29. M. Aragona *et al*., A mechanical checkpoint controls multicellular growth through YAP/TAZ regulation by actin-processing factors. *Cell* **154**, 1047–1059 (2013). doi: 10.1016/j.cell.2013.07.042; pmid: 23954413
30. D. Serra *et al*., Self-organization and symmetry breaking in intestinal organoid development. *Nature* **569**, 66–72 (2019). doi: 10.1038/s41586-019-1146-y; pmid: 31019299
31. I. Lukonin *et al*., Phenotypic landscape of intestinal organoid regeneration. *Nature* **586**, 275–280 (2020). doi: 10.1038/s41586-020-2776-9; pmid: 33029001
32. F. Fan *et al*., Pharmacological targeting of kinases MST1 and MST2 augments tissue repair and regeneration. *Sci. Transl. Med.* **8**, 352ra108 (2016). doi: 10.1126/scitranslmed.aaf2304
33. E. A. Rosado-Olivieri, K. Anderson, J. H. Kenty, D. A. Melton, YAP inhibition enhances the differentiation of functional stem cell-derived insulin-producing β cells. *Nat. Commun.* **10**, 1464 (2019). doi: 10.1038/s41467-019-09404-6; pmid: 30931946
34. Y. Liu-Chittenden *et al*., Genetic and pharmacological disruption of the TEAD-YAP complex suppresses the oncogenic activity of YAP. *Genes Dev.* **26**, 1300–1305 (2012). doi: 10.1101/gad.192856.112; pmid: 22677547
35. W. R. Legant *et al*., Measurement of mechanical tractions exerted by cells in three-dimensional matrices. *Nat. Methods* **7**, 969–971 (2010). doi: 10.1038/nmeth.1531; pmid: 21076420
36. H. F. Farin *et al*., Visualization of a short-range Wnt gradient in the intestinal stem-cell niche. *Nature* **530**, 340–343 (2016). doi: 10.1038/nature16937; pmid: 26863187
37. X. Yin *et al*., Niche-independent high-purity cultures of Lgr5$^+$ intestinal stem cells and their progeny. *Nat. Methods* **11**, 106–112 (2014). doi: 10.1038/nmeth.2737; pmid: 24292484
38. A. E. Shyer, T. R. Huycke, C. Lee, L. Mahadevan, C. J. Tabin, Bending gradients: How the intestinal stem cell gets its home. *Cell* **161**, 569–580 (2015). doi: 10.1016/j.cell.2015.03.041; pmid: 25865482
39. J. Holmberg *et al*., EphB receptors coordinate migration and proliferation in the intestinal stem cell niche. *Cell* **125**, 1151–1163 (2006). doi: 10.1016/j.cell.2006.04.030; pmid: 16777604
40. M. Genander *et al*., Dissociation of EphB2 signaling pathways mediating progenitor cell proliferation and tumor suppression. *Cell* **139**, 679–692 (2009). doi: 10.1016/j.cell.2009.08.048; pmid: 19914164
41. E. Batlle *et al*., β-catenin and TCF mediate cell positioning in the intestinal epithelium by controlling the expression of EphB/ephrinB. *Cell* **111**, 251–263 (2002). doi: 10.1016/S0092-8674(02)01015-2; pmid: 12408869
42. R. Kiesslich *et al*., Local barrier dysfunction identified by confocal laser endomicroscopy predicts relapse in inflammatory bowel disease. *Gut* **61**, 1146–1153 (2012). doi: 10.1136/gutjnl-2011-300695; pmid: 22115910
43. J. J. Liu *et al*., Mind the gaps: Confocal endomicroscopy showed increased density of small bowel epithelial gaps in inflammatory bowel disease. *J. Clin. Gastroenterol.* **45**, 240–245 (2011). doi: 10.1097/MCG.0b013e3181fbdb8a; pmid: 21030873
44. F. Wang *et al*., Active deformation of apoptotic intestinal epithelial cells with adhesion-restricted polarity contributes to apoptotic clearance. *Lab. Invest.* **91**, 462–471 (2011). doi: 10.1038/labinvest.2010.182; pmid: 21042290
45. Y. Guan *et al*., Redistribution of the tight junction protein ZO-1 during physiological shedding of mouse intestinal epithelial cells. *Am. J. Physiol. Cell Physiol.* **300**, C1404–C1414 (2011). doi: 10.1152/ajpcell.00270.2010; pmid: 21346149
46. A. M. Marchiando *et al*., The epithelial barrier is maintained by in vivo tight junction expansion during pathologic intestinal epithelial shedding. *Gastroenterology* **140**, 1208–1218.e1 (2011). doi: 10.1053/j.gastro.2011.01.004; pmid: 21237166
47. C. M. Nelson, Geometric control of tissue morphogenesis. *Biochim. Biophys. Acta Mol. Cell Res.* **1793**, 903–910 (2009). doi: 10.1016/j.bbamcr.2008.12.014


## ACKNOWLEDGMENTS

We thank F. Radtke and U. Koch for providing intestine from Hes1-GFP mice and S. Hoehnel for help with establishing intestinal crypt surfaces. **Funding:** This work was funded by support from the Swiss National Science Foundation (SNSF) research grant 310030_179447, the EU Horizon 2020 Project INTENS (#668294-2), the PHRT - PM/PH Research Project Proposal 2017, Ecole Polytechnique Fédérale de Lausanne (EPFL), and NIH (R01DK120921). N.G. was supported in part by an EMBO Long-Term Postdoctoral Fellowship. T.B. was supported by fellowships from the NSF GRFP and NIH (T32 GM-065103). F.D. was supported in part by the Center for Integrated Nanotechnologies, a US Department of Energy Office of Basic Energy Sciences user facility. Sandia National Laboratories is a multimission laboratory managed and operated by National Technology and Engineering Solutions of Sandia LLC, a wholly owned subsidiary of Honeywell International Inc., for the US Department of Energy National Nuclear Security Administration under contract DENA0003525. **Author contributions:** N.G. and M.P.L. conceived the study, designed experiments, analyzed data, and wrote the manuscript. N.G. was involved in performing and analyzing all experiments in the manuscript except for those involving macroscopic intestinal surfaces. M.N. designed, performed, and analyzed experiments with microtissues and engineered intestinal surfaces and helped in figure preparation. T.B. designed, performed, and analyzed gel photopatterning experiments. O.M. designed, performed, and analyzed experiments with human intestinal microtissues. N.B. developed initial microfabrication approaches for engineered intestinal surfaces. F.W.D. performed mechanical characterization of photopatterned

hydrogels. F.M.Y. performed and analyzed gel photopatterning experiments. P.L. designed and analyzed experiments related to the mechanism of intestinal patterning and provided feedback on the manuscript. K.S.A. designed the materials and concepts for photo-controlled symmetry breaking, including design of experiments and data analysis. All authors read and provided feedback on the manuscript. **Competing interests:** Ecole Polytechnique Fédérale de Lausanne (with M.P.L., N.G., M.N., and N.B.) has filed patent applications pertaining to organoid culture methods described in the paper. **Data and materials availability:** All data are available in the main text or the supplementary materials.

## SUPPLEMENTARY MATERIALS

science.org/doi/10.1126/science.aaw9021
Materials and Methods
Figs. S1 to S12
References (*48*–*51*)
Movies S1 to S8
MDAR Reproducibility Checklist

View/request a protocol for this paper from *Bio-protocol*.

4 February 2019; resubmitted 23 November 2020
Accepted 11 November 2021
10.1126/science.aaw9021